Hydrol. Earth Syst. Sci. Discuss., 11, 4311–4363, 2014
www.hydrol-earth-syst-sci-discuss.net/11/4311/2014/
doi:10.5194/hessd-11-4311-2014

Hydrology and Earth System Sciences
Open Access
Discussions

Large-scale quantification of suspended sediment transport and deposition in the Mekong Delta

N. V. Manh[1], N. V. Dung[1,2], N. N. Hung[2], B. Merz[1], and H. Apel[1]

[1]GFZ – German Research Center for Geoscience Section 5.4 Hydrology, Potsdam, Germany
[2]Southern Institute of Water Resources Research SIWRR, Ho Chi Minh City, Vietnam

Received: 24 February 2014 – Accepted: 9 April 2014 – Published: 17 April 2014

Correspondence to: N. V. Manh (manh@gfz-potsdam.de)

Published by Copernicus Publications on behalf of the European Geosciences Union.

Abstract

Sediment dynamics play a major role for the agricultural and fishery productivity of the Mekong Delta. However, the understanding of sediment dynamics in the Mekong Delta, one of the most complex river deltas in the world, is very limited. This is a consequence of its large extent, the intricate system of rivers, channels and floodplains and the scarcity of observations. This study quantifies, for the first time, the suspended sediment transport and sediment-nutrient deposition in the whole Mekong Delta. To this end, a quasi-2-D hydrodynamic model is combined with a cohesive sediment transport model. The combined model is calibrated automatically using six objective functions to represent the different aspects of the hydraulic and sediment transport components. The model is calibrated for the extreme flood season in 2011 and shows good performance for the two validation years with very different flood characteristics. It is shown how sediment transport and sediment deposition vary from Kratie at the entrance of the Delta to the coast. The main factors influencing the spatial sediment dynamics are the setup of rivers, channels and dike-rings, the sluice gate operations, the magnitude of the floods and tidal influences. The superposition of these factors leads to high spatial variability of sediment transport, in particular in the Vietnamese floodplains. Depending on the flood magnitude, the annual sedimentation rate averaged over the Vietnamese floodplains varies from 0.3 to 2.1 kg m^{-2} yr^{-1}, and the ring dike floodplains trap between 1 and 6 % of the total sediment load at Kratie. This is equivalent to 29 × 10^3–440 × 10^3 t of nutrients (N, P, K, TOC) deposited in the Vietnamese floodplains. This large-scale quantification provides a basis for estimating the benefits of the annual Mekong floods for agriculture and fishery, and is important information for assessing the effects of deltaic subsidence and climate change related sea level rise.

1 Introduction

The Mekong Delta (MD) is critical to the livelihoods and food security of millions of people in Vietnam and Cambodia. It is known as "rice bowl" of South East Asia and one of the world's most productive fisheries. This is a consequence of huge floodplains and wetlands, high local flow variability and the high sediment-nutrient load of the Mekong. However, the Mekong is facing sediment starvation caused by the massive development of hydropower dams (Lu and Siew, 2006; Fu and He, 2007; Fu et al., 2008; Kummu and Varis, 2007; Kummu et al., 2010; Walling, 2008; Gupta et al., 2012; Liu and He, 2012; Liu et al., 2013). The dams planned or already under construction along the main stem of the Mekong in the middle Mekong basin might alter the sediment regime of the MD considerably. The hydropower reservoirs could trap 67 % of the sediment, in case all the planned dams are built (Kummu et al., 2010). Moreover, the MD is sinking due to human activities (Ericson et al., 2006; Syvitsky and Saito, 2007; Syvitsky et al., 2009; Syvitsky and Higgins, 2012). Taking into account the future reduction in sediment load of the Mekong, subsidence rates of $6\,\mathrm{mm\,yr^{-1}}$ have been estimated (Syvitsky, 2009). Understanding and quantifying the sediment and associated nutrient transport and deposition are crucial for the economy of the MD. This knowledge would enable to estimate the benefits of the annual floods, supplying sediment and nutrients for fisheries and a natural fertilization of the agriculturally used floodplains. It would provide a quantitative base for the ongoing debate on the sustainability of the recent and increasing practice of totally blocking floodplain inundation in the Vietnamese part of the MD in favor of three cropping periods per year. Due to the lack of natural fertilization by floods, this cropping practice requires mineral fertilizers (Ve, 2009). Further, it would allow assessing the contribution of sediment deposition to counteract deltaic subsidence and climate change related sea level rise.

So far, the understanding of sediment and nutrient transport and deposition in the MD is very limited. Regarding larger scale sediment transport and deposition only one study has been published using a combination of 1-D, 2-D and 3-D hydrodynamic

models (MRCS/WUP-FIN, 2007). However, the study was limited to the Plain of Reeds (PoR, the north-eastern part of the Vietnamese MD), and considered only the main rivers and channels. On the plot scale, a few experimental studies targeting specific aspects exist. These include fine sediment dynamics in the Mekong estuaries (Wolanski, 1996), fine sediment transport and deposition in the Long Xuyen Quadrangle (Thuyen, 2000), sediment deposition and erosion in floodplains (Hung et al., 2014a, b), and sediment-nutrient deposition in floodplains (Vien et al., 2011; Manh et al., 2013). None of the published studies provides a quantification of the spatial distribution of sediment transport and deposition for the whole MD.

The dense and complex system of rivers, channels and floodplains and the high degree of human interference in the floodplains lead to highly variable patterns of sediment transport and deposition. This heterogeneity poses, in combination with the large spatial extent of the MD, a particular challenge for the quantification of sediment transport and deposition. The Vietnamese part of the MD (VMD) consists of several thousand floodplains, with varying size from approximately 50 to 500 ha. Whereas the Cambodian floodplains are in a natural state, the VMD floodplains are heavily modified. Typically, they are enclosed by a ring dike which is surrounded by a ring channel. Hydraulic structures (sluice gates, pumps) link the floodplains to the channels. The hydraulic connection between channels and floodplains in the VMD varies depending on dike level, flood magnitude and sluice gate and pump operations (Hung et al., 2012), causing a very high variability of floodplain sedimentation (Manh et al., 2013).

Recently, a quasi-2-D hydrodynamic model of the whole MD has been developed by Dung et al. (2011) using DHI Mike 11. This model provides an appropriate compromise between model complexity, spatial coverage and resolution, and computational demand. The model includes a 1-D representation of the river and channel network and a quasi-2-D representation of the VMD floodplains. The floodplains are represented as orthogonal wide and shallow cross sections separated from the channels by dikes and connected to the channels by control structures such as sluice gates. By this approach the floodplain compartments in the VMD are represented in two dimensions

but calculated as 1-D model. The natural floodplains in Cambodia are represented by the 1-D model with extended river cross sections.

To quantify the sediment transport and deposition in the whole MD, this study builds on the work of Dung et al. (2011) and couples the hydraulic model of the MD with a cohesive sediment transport model. The combined model is automatically calibrated with six objectives: daily water levels at 13 stations, daily discharges at 10 stations, inundation extent in the floodplains for several points in time, daily suspended sediment concentrations (SSC) at 2 river stations, SSC at 79 stations for 6 points in time, and annual cumulative sedimentation masses collected at 11 stations in floodplains. Hence, comprehensive data are used for calibration encompassing main rivers, channels and floodplains. The model is applied to three flood events, including an extremely low flood (2010), an average flood (2009) and an extremely high flood (2011).

This combined model and the data from a measurement campaign of sediment-nutrient deposition in the VMD floodplains (Manh et al., 2013) allow for the first time (1) to understand and quantify the spatial distribution of sediment transport and deposition in the whole MD, and (2) to estimate the sediment-nutrient deposition in the floodplains of the VMD.

2 Study area

The Mekong Delta starts at Kratie, Cambodia (Fig. 1). Floods in the MD are generated from the tenth-largest river discharge in the world (Gupta, 2008). The Mekong River drains an area of 795 000 km^2 from the eastern watershed of the Tibetan Plateau to the MD. The Mekong River has a length of 4909 km and passes through three provinces of China, Myanmar, Lao PDR, Thailand, Cambodia and Vietnam before emptying into the South China Sea. The annual flood pulse in response to the Western North-Pacific monsoon during the months July to October is the key hydrological characteristic of the Mekong River. The start of the flood season in the MD is usually defined when the mean annual discharge of 13 600 $m^3 s^{-1}$ at Kratie is exceeded

(MRC, 2007). The long-term average of annual flood volume is 330 km^3 and the mean annual flood duration is 137 days starting typically in July (MRC, 2011a). The estimated annual sediment load of the Mekong varies between 50 and 160 million tons (Lu al et., 2013: 50–91 million tons; Milliman and Farnsworth, 2011: 110 million tons; Walling, 2008: 160 million tons). The annual dissolved sediment load was estimated to 60 million tons by Milliman and Farnsworth (2011).

To facilitate the discussion of flooding and sediment transport, the MD can be divided into the four subsystems: (1) Cambodian Mekong Delta, (2) Tonle Sap, (3) Vietnamese Mekong Delta and (4) coastal area (Fig. 1, Fig. 5, right panel). In the following, the salient features of each subsystem are introduced.

The subsystem "Cambodian Mekong Delta" consists of all rivers and floodplains in Cambodia excluding the Tonle Sap. The Mekong River downstream of the station Kratie until the Mekong is divided into three branches at the Chatomuk conjunction near Phnom Penh: the Tonle Sap River diverting water north to the Tonle Sap Lake (TSL) in Cambodia, and two branches transporting water south to the sea, namely the Bassac River (Hau River in Vietnam) and the Mekong River (Tien River in Vietnam). These floodplains with a size of around 11 000 km^2 are in a natural state. During flood seasons overbank flow from the Mekong and Bassac Rivers inundates them.

The subsystem "Tonle Sap" includes the Tonle Sap Lake and Tonle Sap River. The flow into the Tonle Sap Lake is reversed at the end of the flood season; hence the TSL retains flood water and sediment during the flood season. TSL stores up to 10 % of the total wet season flow volume of Kratie, and reduces the maximum discharge of Kratie by 16 % (MRC, 2009).

The subsystem "Vietnamese Mekong Delta" stretches from the stations Tan Chau and Chau Doc to the stations My Thuan and Can Tho at the Tien River and Hau River, respectively, with an area of about 19 500 km^2. The VMD is known as the most complex river delta in the world as a result of the immense anthropogenic interference encompassing numerous man-made channels, dikes, sluices gates and pumps. The total length of the channel network is about 91 000 km, resulting approximately in the

doubled length of the dike system. 75 % of the ≅ 1 million people in the VMD live in rural areas (statistical data in 2011), whereas the rural residential areas are preferably distributed along the dike lines. Most of the transportation during the flood season uses the waterways, especially in high flood events. The main channels are directly connected to the Mekong River and the Bassac River. Secondary channels distribute water from the main channels to floodplains and smaller channels. The floodplains are thus dissected into numerous, mostly rectangular compartments, which are typically enclosed by dike rings of different height.

The floodplains of the VMD are typically subdivided into 3 regions (Fig. 1): (1) the Long Xuyen Quadrangle (LXQ), an area of annually inundated floodplains bordering Cambodia and stretching west of the Hau River to the coast, (2) the Plains of Reeds (PoR), an area of annually inundated floodplains also bordering Cambodia but to the East of the Tien River, and (3) the area in between Tien River and Hau River (THA). The inundations in LXQ are mainly caused by the Hau River and to a small fraction by overland flow from the Cambodian floodplains. In PoR, floods are caused by the Tien River and by a significant amount of overland flow from the Cambodian floodplains providing a second flood pulse, typically with some weeks delay to the peak flow of the Hau River.

Almost all floodplains in VMD are compartmented and used for agricultural production. The original floodplains are fragmented by the channel network and enclosed by ring dikes. The compartment areas range from 50–500 ha. Compartments are linked to channels through a number of sluice gates. The operation of sluice gates depends on flood magnitudes, ring dike heights and the crop patterns in the compartments. Ring dike systems are usually classified as low or high dike compartments. In high dike compartments the dike level is designed based on the maximum water level of the historical floods of the year 2000. They are equipped with sluice gates and often with additional pumping systems. The flooding of these compartments is usually completely controlled, unless the flood magnitude exceeds the designed crest levels. The total length of the high dike compartments increased rapidly in the past 10 yr. Remote

sensing data show that the triple crop area, an indicator for high dike rings and complete flood control, is concentrated in LXQ and THA (Leinenkugel et al., 2013). In low dike compartments the flood can be controlled during the rising and falling stages of the flood season only. Overbank flow occurs during the high stage of the annual floods. The heights of low dike compartments vary depending on the experience and capacity of land owners. In a normal flood year, the remaining ponding water in these compartments is pumped out at the end of November to plant the dry season crop. In years of extreme or damaging floods, the water volume may exceed the pumping capacity and the dry season crop is cancelled, as e.g. in 2011.

The subsystem “Coastal area” extends from downstream of My Thuan gauging station at the Tien River and downstream of Can Tho station at the Hau River to the sea. In this area tidal backwater effects can be observed throughout the year.

When considering the flood and sediment processes in the MD, the characteristics of these subsystems and of the flood wave entering the MD need to be considered. Hung et al. (2012) divided the flood season into three periods. In the rising stage and falling stage, the hydraulic situation in the MD is controlled, besides the flow entering the MD at Kratie, also by tide influences and the inflow from the Mekong River into TSL (rising stage) and the reverted flow from TSL to the Mekong (falling stage). The high stage is given when water level in the Mekong River is high enough to counterbalance the water level of the TSL and to dampen the tidal backwater effects in the coastal area to a large extent. In addition, the hydraulic regime and sediment dynamics in VMD are strongly influenced by human interferences, and Hung et al. (2012) found a strong influence of the crop schedule on the hydrology of the floodplains.

The typical flood characteristics in the MD are: (1) buffering of the flood pulse by the Tonle Sap Lake, (2) a secondary flood pulse besides the river pulse caused by large-scale overbank flow over the Cambodian floodplains into the VMD, (3) large-scale, annually inundated areas (> 20 000 km^2), (4) extended inundation periods (3–4 months), (5) strong human interference in the hydraulic regime and the suspended sediment transport, particularly in the VMD.

3 Model setup and data

3.1 Description of the 1-D hydrodynamic and sediment transport model

The Mike11 hydrodynamic model (HD) is based on one-dimensional hydrodynamic equations and solves the vertically integrated equations of conservation of continuity and momentum (the "Saint Venant" equations). The solution is based on an implicit finite difference scheme developed by Abbott and Ionescu (1967).

The cohesive sediment transport module of Mike11 is based on the mass conservative 1-D advection-dispersion (AD) equation:

$$\frac{\delta AC}{\delta t} + \frac{\delta QC}{\delta x} - \frac{\delta}{\delta x}\left(AD\frac{\delta C}{\delta x}\right) = -AKC + C_2 q \quad (1)$$

where C is the concentration, D is the dispersion coefficient, A the cross-sectional area, K the linear decay coefficient, C_2 the source/sink concentration, q the lateral inflow, x the space coordinate and t the time coordinate. The main assumptions are: (1) the considered substance is completely mixed over the cross sections implying that a source/sink term is considered to mix instantaneously over the cross section; (2) Fick's diffusion law applies, i.e. the dispersive transport is proportional to the concentration gradient.

The falling velocity of sediment flocs mainly depends on the sediment concentration:

$$W_S = k(1 - VC)^\gamma \text{ with } k = \frac{W_0(1 - VC)^\gamma}{VC^m} \quad (2)$$

where W_S is the settling velocity of flocs ($\mathrm{m\,s^{-1}}$), VC is the volume concentration of suspended sediment ($\mathrm{m^3\,m^{-3}}$), m, γ are empirical coefficients and W_0 is the free settling velocity that is determined by the sediment grain size considering the observed cohesive sediment properties (Sect. 3.3).

The deposition process is described as:

$$S_d = \frac{W_S \mathrm{SSC}}{h_*}\left(1 - \frac{\tau_b}{\tau_{c,b}}\right) \text{ for } \tau_{c,b} > \tau_b = \rho g \frac{V^2}{h^{\frac{1}{3}}}\left(\frac{1}{n}\right)^2 \quad (3)$$

where S_d is deposition rate ($\mathrm{kg\,m^{-3}\,s^{-1}}$) describing the source/sink term in the advection-dispersion equation. W_S is the floc settling velocity ($\mathrm{m\,s^{-1}}$), SSC is suspended sediment concentration ($\mathrm{kg\,m^{-3}}$), h_* is the average depth through which the particles settle (m), τ_b and $\tau_{c,b}$ are bed shear stress and critical bed shear stress for deposition ($\mathrm{N\,m^{-2}}$), ρ is the fluid density ($\mathrm{kg\,m^{-3}}$), g the acceleration of gravity ($\mathrm{m\,s^{-2}}$), n is the Manning number, h the flow depth (m) and V the flow velocity ($\mathrm{m\,s^{-1}}$).

The mass in grid point j is given as:

$$M_j = \mathrm{vol}_j \mathrm{SSC}_j \quad (4)$$

where M is the mass at given time at given grid point j (kg), SSC is suspended sediment concentration ($\mathrm{kg\,m^{-3}}$) and vol is the volume of grid point j.

3.2 Approach for hydrodynamic and sediment transport modelling in the MD

The quasi-2-D hydrodynamic model developed by Dung et al. (2011) is applied to simulate the flood propagation and inundation in the MD from Kratie to the coast including the Tonle Sap Lake. Figure 2a shows the representation of the MD by the hydrodynamic model. In Fig. 2b the quasi-2-D representation of the floodplain compartments is illustrated. A floodplain is enclosed by main and/or secondary channels. The floodplain itself is represented by "virtual" channels with wide cross sections extracted from the SRTM DEM. Defining four virtual intersecting channels per compartment, a quasi-2-D simulation of the floodplain is enabled. The cross section width of each virtual channel is defined in such a way that the compartment area is preserved. Details can be found in Dung et al. (2011).

The crest levels of the dikes are modeled as sill levels of sluice gates in each floodplain compartment in the model. The width of the sluice gates in the model is either the width of sluice gates actually present for high dike compartments, or 50 m for low dikes. The dike crest levels are given by the sill levels of the control structures. Data about dikes and control structures were collected by Dung et al. (2011) from different local and regional authorities.

The multi-objective calibration of Dung et al. (2011) revealed systematic errors in the dike crest levels implemented in the model, probably caused by different vertical reference values of the collected dike data. Thus the model dike heights are updated based on an analysis of water masks from satellite images (Kuenzer al et., 2013) combined with maximum simulated water levels from the hydraulic model (Dung et al., 2011). The dike levels of floodplain compartments are corrected by comparing the maximum simulated water levels the with maximum observed flood extents for three flood seasons: the average flood of 2009, the exceptionally low flood of 2010 and the extreme flood 2011. Dike heights are corrected as follows:

- No inundation during all three floods: these compartments are fully controlled, high dike compartments. Model dike heights are set higher than the maximum simulated water levels of the surrounding channels. These dike compartments are concentrated in THA and LXQ.
- Inundation during the high stage of all three floods, but no inundation during the rising and falling stages: these compartments are low dike compartments. Dike heights are refined based on the simulated water levels in the surrounding channels during the rising stage and/or falling stage. These compartments can be found everywhere in VMD but are concentrated in PoR.
- No inundation during the high stage of the low and average flood, but inundated during the extreme flood: these compartments work as high dike compartments during small and normal floods and as low dike compartments during extreme floods. Dike heights are defined within the range of maximum simulated water levels in the extreme and normal flood.

In the MD only a small number of the sluice gates have real radial or vertical gates, whereas most of the sluice gates are operated by movable high sills using sandbags. The opening time is decided by the land owner depending on the rice crop schedule and the flood magnitude. In the model the operation of real sluice gates is controlled by the water level of the incoming flow and/or a fixed schedule. Data on the operation of these sluice gates was collected from authorities by Dung et al. (2011). The remaining sluice gates are modeled as broad crested weirs, for which sill level data were collected from authorities (Dung et al., 2011) or estimated from the comparison of simulated water levels and observed water extent as described above. Pumping stations are excluded in the model because the pumps are operated at the end of the flooding period to drain the compartments for the new crop. In this period, SSC is very low and the effects of pumping can be neglected for the estimation of floodplain deposition.

The model contains 2340 hydraulic structures consisting of weirs, culverts and sluice gates. This complexity is a challenge for the stability of the cohesive sediment transport model. Hence, the model network of Dung et al. (2011) is slightly modified to satisfy the stability conditions based on the Courant ($Cr = v\frac{\Delta t}{\Delta x} < 2$) and Péclet number ($Pe = v\frac{\Delta x}{D} > 2$) (Mike11, 2012). Numerical stability can be achieved by increasing the distance between the computational points Δx to satisfy both Courant and Péclet stability criteria, and by decreasing the time step Δt to satisfy the Courant criterion. Hence, the cross section spacing is increased whereby the important elements influencing the hydraulic conditions (e.g. topography, location of hydraulic structures) are taken into account. A minimum Δx of 700 m and a time step Δt of the sediment transport model of 3–5 min are chosen. This setup results in model run times of 7–12 h for one flood season. Hence, numerical stability of the hydrodynamic and sediment transport model is given and automatic model calibration is feasible.

The sediment dynamics in the floodplains are strongly influenced by local resuspension due to human activities (Manh al et., 2013). The sediment deposition in

floodplains includes not only watershed sediment from upstream but also locally eroded sediment. In order to quantify the net delivered sediment-nutrient from the watershed, the disturbances from human activities in the MD are ignored. A very high critical shear stress for erosion is used in the model to ensure that no erosion occurs in the river network.

3.3 Model parameterization

The model parameters are the roughness coefficient (n) for the HD model, and the longitudinal dispersion coefficient (D), the free settling velocity (W_0) and the critical shear stress for deposition (τ_d) for the AD model. In order to reduce the degrees of freedom in the parameter estimation, the MD is divided into eleven parameter zones (Table 1), for which the calibration parameters are assumed to be constant. This zonation is a refinement of the zones used by Dung et al. (2011), taking into account the different characteristics of main rivers, channels and floodplains. To further reduce the calibration effort, not all calibration parameters are calibrated in all eleven zones. Depending on the parameter sensitivity and the flow characteristics, some parameters are fixed in some zones (Table 1).

The Manning roughness coefficient n is calibrated in ten zones. The range of n in the calibration is set to 0.016–0.10. In the coastal zone wherein the rivers are very straight, bed material is mostly deposited clay and flow is governed by the tide, n is set to 0.016. The longitudinal dispersion coefficient D controls the dispersive sediment transport. It represents the influence of the non-uniform flow velocity distribution. The dispersion coefficient is determined as a function of the mean flow velocity: $D = a|V|^b$ is flow velocity V and constants a, b. Model runs showed that the suspended sediment moving with the velocity of water (advection) is orders of magnitude higher than the spreading due to non-homogeneous velocity distribution (dispersion). Thus, to reduce to complexity of the calibration, we fix $b = 1$ for the whole MD and calibrate a (dispersion factor) for the areas with high variability of flow velocity (channels in the VMD and coastal zone, Table 1). The a values in other areas are fixed based on equivalent

mean flow velocities and dispersion coefficients of 81 measurements in 30 US rivers (Kashefipour al et., 2002).

The value for free settling velocity (W_0) is based on recent studies on suspended sediment and sedimentation in the MD. Manh et al. (2013) analyzed sediment deposition at 11 sites over the VMD and found that the sediment dispersed grain size and nutrient content are uniformly distributed over the study sites, with a sediment grain size distribution of 41 % clay (grain size $< 2\,\mu m$) and 51 % silt (grain size 2–63 µm). Moreover, it has been observed that the sediment is cohesive and transported primarily in a flocculated state (Droppo, 2001). In the model the floc settling velocity W_S is calculated based on Eq. (2) in which W_0 is specified based on dispersed grain size from measurements. In floodplains in PoR, Hung et al. (2014b) found dispersed grain sizes from 12 sediment traps in the range of D_{50} = 10–15 µm. Wolanski (1996) analyzed dispersed grain size of bottled samples with D_{50} = 2.5–3.9 µm in the freshwater region of the Hau River estuary. MRC/DMS (2010) measured $D_{50} \cong$ 3–8 µm in the Tonle Sap River and even finer in TSL. The reported grain sizes D_{50} = 2.5–15 µm are equivalent to free settling velocities $W = 2.5 \times 10^{-4}$–$1 \times 10^{-5}\,m\,s^{-1}$ using Stoke's law with average measured water temperature $t \cong 30^{\circ}C$ (Hung et al., 2014b). Furthermore, Hung et al. (2014b) derived the deposition shear stress τ_d = 0.021–0.029 $N\,m^{-2}$ and floc grain size D_{50} = 35 µm by inverse modeling, yielding the best sediment deposition estimation. This estimation is quite similar to the measurements by Wolanski et al. (1996) and MRC/DMS (2010). Thus the free settling velocity W_0 and the deposition shear stress τ_d derived by Hung (2014b) are used as parameter ranges in the calibration.

A sensitive analysis was performed to determine which parameter can be set constant in which zone. 300 Monte Carlo runs were performed with the AD model by fixing the dispersion coefficient D and τ_d or W_0 to determine the sensitivity of W_0 and τ_d in each zone. In the zones with low sensitivities of the parameters W_0 or τ_d, this parameter was fixed based on the studies mentioned above. The calibration range of W_0 and τ_d in the remaining zones is 1×10^{-3}–$1 \times 10^{-5}\,m\,s^{-1}$ and 0.01–0.2 $N\,m^{-2}$, respectively.

The fixed and calibrated parameter values (result of Sect. 4) of τ_d and W_0 for specific zones are shown in Table 1.

3.4 Measurement data

The measured data used for calibration and validation encompass water level, discharge, inundation extent, SSC in main rivers, SSC in channels, and floodplain sediment deposition. The first three variables are used to calibrate the hydrodynamic module, while the latter three variables are used for sediment transport calibration. The flood in 2011 serves as calibration period, because the floodplain deposition data was collected in 2011 (Manh et al., 2013).

Daily water level and discharge data were collected for 18 stations. They include 5 stations in the main rivers with both discharge and water level (Tan Chau, Chau Doc, Can Tho, My Thuan, Vam Nao) and additionally 7 water level stations and 5 discharge stations in main channels (Fig. 2). For the evaluation of the spatial performance of the hydrodynamic model water masks derived from optical MODIS satellite images are used. The simulated inundation extents are calibrated against these water masks.

For the calibration of the sediment transport SSC data from 79 locations were acquired from the Southern Regional Hydro-Meteorological Center of Vietnam. These measurements were conducted manually every 15 days during the flood period by grab water samples and suspended sediment mass quantification by filtering and drying. The sediment deposition in the compartments of the VMD of the complete flood season 2011 was monitored by Manh et al. (2013), deploying a large number of sediment traps. This study provided mean cumulative sedimentation rates including an uncertainty range for 11 compartments distributed over PoR and LXQ.

In addition, Manh et al. (2013) determined the nutrient fractions of the sediment deposited in the sediment traps. The analyzed nutrients are Total Nitrogen (TN), Total Phosphorus (TP), Total Potassium (TK) and Total Organic Carbon (TOC). The sedimentation mass fractions of these nutrients varied only slightly in space. Thus the nutrient content of the sediment can be estimated by the average fraction of 6.7 %.

This value defines the total deposition of TN, TP, TK, and TOC as fraction of deposited sediment, and is used to estimate the nutrient deposition in the floodplains of the VMD. The deposition of the different nutrients is derived by the following fractions: TN = 4.9 %, TP = 1.9 %, TK = 22.5 % and TOC = 70.7 % of the total nutrient deposition.

3.5 Definition of the sediment model boundary conditions

The simulation of sediment dynamics requires specifying SSC for the upper and lower model boundary at daily resolution. However, daily SSC data are neither for the upper model boundary nor for the lower boundary available. Hence, daily SSC are reconstructed using lower-resolution SSC data.

For the upper model boundary, daily SSC time series are derived from daily discharge and monthly or sporadic SSC data of the Mekong River at Kratie and neighboring gauging stations. In this analysis, however, one has to consider the reported low quality of the available SSC data (Walling et al., 2005). Before 2010 only monthly observations of water quality including total suspended solid (TSS) at Kratie are available. TSS was measured taking a single water sample at 0.8 m depth, which is a very rough and possibly strongly biased estimation of the average SSC over the whole river cross section. Recently, the Mekong River Commission (MRC) measured SSC as the average of 5 vertical profiles over the cross section at Kratie. The measurements were taken on 6 dates (every 2 months) in 2010 and on 20 dates from June to December 2011. The reconstruction of daily SSC at Kratie is based on this data set.

Most often, SSC is reconstructed using a sediment rating curve. The 26 measurements at Kratie are significantly correlated to discharge (significance level < 0.05) with a Spearman's rank correlation coefficient of $\rho = 0.79$. A sediment rating curve is constructed using a second order logarithm power function:

$$SSC_t^{Krat} = 10^{\left(-494.02 \lg\left(Q_t^{Krat}\right)^{-4.52} + 2.88\right)} \quad (5)$$

in which SSC_t^{Krat} is SSC ($mg\,L^{-1}$) at time t at Kratie, Q_t^{Krat} is discharge ($m^3\,s^{-1}$) at time t at Kratie. The rating curve is shown in Fig. 3a.

Another possibility to reconstruct SSC at Kratie is to correlate SSC at Kratie to SSC measurements at a nearby station with longer daily time series. Considering that the suspended sediment in the MD is very fine (Manh et al., 2013) and that no significant lateral SSC input downstream of Kratie exists, except the flow from TSL, the measured daily SSC at Tan Chau and Chau Doc in Vietnam (see locations in Fig. 1) might be used to reconstruct daily SSC at Kratie. An analysis of the SSC data of Tan Chau and Chau Doc shows that, due to the hydraulic properties of the flow diversion of the Mekong into Mekong, Bassac and Tonle Sap Rivers, the flow into and from TSL influences mainly the SSC in the Bassac River at Chau Doc station (Fig. 4b). Hence, the daily SSC records of Tan Chau at the Mekong River are used as predictor for SSC in Kratie. The average travel time from Kratie to Tan Chau is 1–2 days, which is considered as lag in the correlation analysis. We found a close linear correlation ($R = 0.95$) of the measured SSC at Kratie to SCC at Tan Chau with a 1 day lag. The linear regression is given as:

$$SSC_t^{Krat} = 1.1 SSC_{t+1}^{TC} + 12.77 \quad (6)$$

in which SSC_t^{Krat} is SSC ($mg\,L^{-1}$) at time t at Kratie, SSC_{t+1}^{TC} is SSC ($mg\,L^{-1}$) at time $t+1$ at Tan Chau. It is noteworthy that the same SSC measurement method is applied at both stations. Figure 3b shows the regression of SSC_{t+1}^{TC} vs. SSC_t^{Krat} along with the confidence bounds.

The derived SSC time series at Kratie based on these two methods yield very similar total sediment loads (106 mil. ton for the rating curve, and 107 mil. ton for the linear regression to Tan Chau), however, the SSC time series derived by the rating curve method is rather smooth and does not capture the SSC peaks existing in the measurements of Tan Chau. Hence, the rating curve method seems to suppress some fraction of the SSC variability (Fig. 3c). Further, the regression based method provides smaller uncertainty bounds (Fig. 3d). Based on these two arguments, the regression based method is used to reconstruct daily SSC at the upper model boundary.

For the definition of the lower boundaries at the river mouths remote sensing data are used. Water turbidity was derived from multi-sensor satellite scenes. The turbidity was then calibrated against in-situ SSC measurements. This provided approximately weekly SSC values at the various river mouths. These values are linearly interpolated to daily SSC. Details of the image processing and validation can be found in Heege et al. (2014).

4 Model calibration and validation

Model calibration and validation cover an extreme event (2011), a normal event (2009) and a low flood event (2010). 2011 was the most severe flood in recent times with a peak discharge in Kratie of $63 \times 10^3\,m^3\,s^{-1}$, which is higher than the historically most damaging flood in 2000. In terms of flood volume, this event is the third largest one in the observation period of 88 yr (MRC, 2011b). In 2010, the lowest flood volume ever was recorded, the flood peak was $37 \times 10^3\,m^3\,s^{-1}$, and the flood lasted 6 weeks less than on average (MRC, 2011a). 2009 was an average flood both in terms of peak discharge and volume (MRC, 2010). The calibration is performed for the extreme flood in 2011, because for this year the most comprehensive data including floodplain deposition is available. The model is validated against the data of 2009 and 2010. Hence, the model is calibrated for an extreme flood and validated against a normal flood and an extremely low flood, thus providing information about the applicability of the model over the possible event magnitude scale.

4.1 Model calibration

To reduce the complexity of the calibration and to reduce the runtime, the hydrodynamic (HD) and sediment transport (AD) model components are run and calibrated individually. The HD simulation results are fed as input into the AD model. This separation has the advantage that different computational time steps can be used for the two

components, dramatically reducing the required runtime. The automatic multi-objective calibration algorithm developed by Dung et al. (2011) and based on the NSGA-II algorithm is applied. This enables an objective calibration considering different optimization objectives.

The HD model is calibrated with three objective functions: discharge in rivers and channels, water level in rivers and channels, and inundation extent. The first two objectives are quantified by the mean Nash–Sutcliffe efficiency (NSE) over all considered gauging stations. The spatial inundation performance is quantified by the Flood Area Index (FAI) comparing the simulated extent with the inundation extent derived from MODIS Terra images. Cloud covered areas in the MODIS images are considered as no-data in both observed and simulated inundation. This multi-objective calibration results in a Pareto optimal set of HD model parameters. From this set we select the set with the least Euclidian distance to the optimal solution.

The AD model is calibrated with three objectives: SSC in main rivers, SSC in the channels and cumulative sedimentation rates on the floodplains. The Nash–Sutcliffe efficiency is used for the first objective, and the root mean square error (RSME) is used for the second and third objectives. RSME is selected because the measurements of channel SSC and sedimentation are not continuous in time. RMSE for cumulative sedimentation rate is calculated for the mean and, in addition, for the 95 % confidence bounds of the observed deposition derived by Manh et al. (2013). The AD model calibration results in another Pareto-optimal set, from which the parameter set with the least Euclidian distance to the optimal solution is selected. The calibration zones and parameters are given in Table 1.

4.2 Model validation

For model validation, the flood seasons 2009 and 2010 are used. Since floodplain sedimentation data (Manh et al., 2013) is available for 2011 only, the data from Hung et al. (2014b) are used for validating sediment deposition. Hung et al. (2014b) also used sediment traps to quantify sedimentation in floodplains in 2009 (2 locations) and

in 2010 (1 location). This data set is much less comprehensive than the data set of Manh et al. (2013), and is limited to a small study site in the PoR. Further, less data for discharge, water level and SSC is available for 2010 compared to 2011 and 2009. This needs to be considered in the interpretation of the validation results.

The calibration and validation results are summarized in Table 2 and Fig. 4a–c. Overall, the validation shows similar results as the calibration. The validation performs better for discharge and SSC in 2010 which is likely due to much less overland flow, reducing the possible errors stemming from erroneous dike levels and floodplain representation. The agreement between simulation and measurements for SSC at Chau Doc in 2009 is very low. This is probably the consequence the poor quality of measured data at Chau Doc station in 2009 as illustrated in Fig. 4b (left panel). Whereas SSC is related to discharge in 2011 for Chau Doc and in 2009 and 2011 for Tan Chau, this coherence between discharge and SSC is frequently not given in 2009 for Chau Doc.

Overall, the model performance indices (Table 2) show a good agreement between simulation and measurements. This is illustrated in Fig. 4a and b, comparing simulated and measured water levels, discharges and SSC at the key stations in the VMD (Tan Chau, Chau Doc, Vam Nao). Sediment deposition is less well simulated. This is discussed in Sect. 5.3.

5 Results and discussion

The presentation of the modeling results is divided into three parts: SSC transport in the whole MD, SSC dynamics on the floodplains of the VDM, and floodplain sediment deposition in the VMD.

5.1 Sediment transport in the Mekong Delta

In the following, the results on SSC transport are given according to the subsystems introduced in Sect. 2. The fluxes of these subsystems are compared to the values at the

upstream boundary Kratie. These results are summarized in Table 3, and the variation of the transported sediment from Kratie to the coast is exemplarily shown for 2009 in Fig. 5.

Rather significant storage of water and sediment occurs in the subsystem "Tonle Sap". The flood volume stored in the TSL ranges from 6 to 12 % compared to the flood volume at Kratie for the three simulated flood events. This is equivalent to 14–55 km^3. These figures compare well with the average value of 41.8 km^3 in the TSL water balance analysis published by Kummu et al. (2014). The total simulated sediment mass input to the TSL is 2.1×10^6 t in 2010, 5.2×10^6 t in 2009 and 10.6×10^6 t in 2011 (Table 3). Since the reverse flow of the TSL to the Bassac River at the end of the flood season has a low SSC, these figures are an estimate of the total sediment loss in the TSL. They compare well with the estimated historical average value of 5.09×10^6 t by Kummu et al. (2008).

In the subsystem "Cambodian Mekong Delta", 24–27 % of the suspended sediment load of the Mekong at Kratie is transported into the Cambodian floodplains, and 4–7 % is further conveyed by overland flow to PoR and LXQ in the VMD. The remaining proportion is deposited in the Cambodian floodplains or returned to the main rivers.

The total sediment transported to the "Vietnamese Mekong Delta" varies from 64 % for the extreme flood to 71 % for the low flood, with a corresponding flood volume of 86 and 93 %, respectively. The largest fraction of the sediment is transported through the stations Tan Chau and Chau Doc, ranging from 57 to 68 % (corresponding flood volume: 78–89 %) for the high and low flood year, respectively. This means the smaller the flood event the higher is the proportion of sediment load passing through Tan Chau and Chau Doc. This has to be attributed to higher sediment trapping in the TSL and the Cambodian floodplains during larger events. Furthermore, it has to be noted that the transport capability of the Mekong River is three to four times greater than the capability of the Bassac River. The differentiation of SSC in the rivers from upstream to downstream is explained by the reduction of SSC in the main rivers by bed sedimentation of coarser grain sizes, and the SSC-dilution effect caused by the return flow from

TSL. The return flow has much lower SSC than the inflow (i.e. the Mekong flow) due to the settlement of sediment in the TSL. As the TSL return flow enters the Bassac branch, SSC at Chau Doc is significant smaller than SSC at Tan Chau during the high and falling stage of flood events. During this period SSC at Chau Doc is approximately 50 % of SSC at Kratie (Fig. 4b).

The transport capacity in Tien River and Hau River is balanced again through the Vam Nao connection. 23–28 % of the overall flood volume and 18–21 % of the sediment load is conveyed from Tien River through the Vam Nao station to Hau River. Downstream of the Vam Nao connection, the Tien and Hau Rivers carry approximately the same suspended sediment load. The total suspended sediment transport to the VMD floodplains varies from 12 % for the low flood to 15 % for the extreme flood. The channels in the VMD floodplains obtain sediment from two sources: the main part stems from the Tien and Hau Rivers and is conveyed through the channel network to PoR and LXQ. The second part originates from the overland flow from the Cambodian floodplains. SSC of the overland flow is lower compared to SSC in the main rivers as consequence of the deposition in the Cambodian floodplains. The VMD floodplain compartments trap 1–6 % of the total sediment load at Kratie. This is equivalent to 9–41 % of total transported sediment into the VMD floodplains.

The remaining suspended sediment is transported to the subsystem "coastal area". In the tidal backwater influenced coastal zone also the fine sediments can be deposited in the river beds (9–11 %). However, the model does not consider salt water intrusion and thus the effects of density layering on sediment deposition. The simulated river bed deposition in the coastal zone can be taken as a rough indication only. Overall, the total sediment load transported to the coastal area at My Thuan and Can Tho ranges from 48 % for the extreme event to 60 % for the low flood.

Figure 5 (left panel) provides an overview of the spatial distribution of sediment transport in the whole MD and Fig. 5 (right panel) shows schematically variation of the sediment load through the MD. The numbers indicate the fraction of sediment transport compared to the sediment load at Kratie. The largest proportion of sediment is kept

in the main rivers and channels. As expected, the sediment loads are not equally distributed in the VMD. Highest SSC value are simulated in and close to the main Mekong branches and along the Cambodian–Vietnamese border (PoR and LXQ), where the channels in the VMD collect the sediment of the overland flow from Cambodia. In the upper VMD the PoR receives higher sediment loads, which are also transported deeper into the floodplain area compared to LXQ. This is caused by three reasons: (1) LXQ is directly influenced by tidal backwater effects from the West Sea reducing flows from the Hau River into the floodplain, (2) SSC in the Hau River is smaller than SSC in the Tien River upstream of the Vam Nao connection, and (3) most of the floodplains with high ring dike systems blocking the inundation of the floodplains are concentrated in LXQ. In THA, the area between Tien and Hau River, almost all floodplains are fully protected by high ring dikes prohibiting floodplain inundation and deposition. Sediment is transported from the Tien River to the Hau River only. In the coastal areas, sediment transport is governed by tidal influences. Most of channels in this area do not receive sediment from the Tien and Hau Rivers because of back and forth flow in these channels.

5.2 Sediment dynamics in the VMD floodplains

In this section the sediment dynamics in the VMD floodplain regions PoR, LXQ and THA are elaborated. These floodplains obtain sediment from two sources: via channels starting from Tien River and Hau River, and via channels collecting overland flow from Cambodia.

During the rising flood stage the bulk of the flow is concentrated in the rivers and channels. Overbank flow into Cambodian floodplains does not yet occur, and flow to TSL occurs mostly through the Tonle Sap River. In the VMD, all floodplain sluice gates are still closed to protect the second rice crop of the year, but also the low dikes prevent extensive flooding of the compartments. Water levels are rising, but in the main rivers and the channel network only. SSC is also rising with the onset of the flood. SSC decreases with distance from the Tien River and Hau River towards the remote parts

of PoR and LXQ (see Fig. 6, left panel and Fig. 7). In both PoR and LXQ, SSC greater than 50 mg L^{-1} can be found up to a distance of 60–70 km from the Tien River and Hau River, also the remote parts of the floodplains show noteworthy SSCs in the channels during all floods (Fig. 6, left panel).

During the high flood stage overbank flow occurs on both sides of the Mekong and Bassac Rivers, and all sluice gates in low dike compartments, but also some of the high dike compartments, depending on the management scheme, are opened after the second rice crop harvest. Later on the low dikes are also overflown. Now the VMD receives flood water from the Tien and Hau Rivers and overland flow from the Cambodian floodplains. The SSC patterns depend on the magnitude of the overflow from the Cambodian floodplains which has significantly smaller SSC. This, in turn, is governed by the overall flood magnitude. In the normal year 2009, floodplain compartments are filled through sluice gates after 2–3 days. This results in a drastic reduction of SSC in the channels due to sediment deposition in the compartments and in low SSC of the return flow from the compartments to the channels (Fig. 6, right panel). Notable SSC are then observed until a distance of 20 km from the main rivers only. SSC in the central and remote parts of the PoR and LXQ is reduced to below 5 mg L^{-1}.

In PoR, 24–37 % of the flood volume stems from the Cambodian floodplains. Overland flow from Cambodia enters the border channels, from where it is redistributed to the channels of the PoR and to the Vam Co River. Flow from the Tien River also enters PoR through channels which are mainly parallel to the border channels. Due to the hydraulic head imposed by the flood water from the Cambodian floodplains, the flow velocities in these channels are comparatively small. During the later period of the high flood stage the flow into PoR from the Tien River might become stagnant or even reverse during low tide. Besides the compartment flooding, this is the reason for the low SSC in the southern part of the PoR in October, even close to the Tien River (Fig. 6, right panel). In LXQ, floodplains receive 25–33 % of the overland flood volume from the Cambodian floodplains. Like in PoR, the border channel redistributes the water to the channels of LXQ and to the West Sea. The difference to PoR is that flood water can

flow directly to the West Sea. Also the overland flood wave is generally lower and thus also the hydraulic head of the overland flood compared to PoR. Because in LXQ the flow from the Hau River is less dampened by the overland flood wave, higher flows and SSC rates occur in the channels of the southern parts of LXQ compared to PoR.

In the falling flood stage the flow is reverted from TSL to the Mekong just upstream of the diversion of the Bassac and Mekong branches. The backflow from TSL has low SSC, thus the SSC in the Mekong is reduced by dilution and considerably lower than during the previous flood stages with similar discharges. This SSC reduction particularly affects the Bassac River branch, where the dilution is more substantial due to incomplete transversal mixing between the confluence of the Tonle Sap River to the Mekong and the diversion of Mekong and Bassac. The small SSC of the Bassac/Hau River is raised again after the Van Nao connection between the Tien and Hau Rivers. SSC of the coastal areas remain unaffected by these processes, because in this region SSC is dominated by tidal backwater effects.

The reduction of SSC with distance to the main rivers and the variation of the reduction during the flood period are illustrated in Fig. 7. It shows the simulated SSC dynamics in 2011 in a typical channel in the VMD, the Hong Ngu channel. It is connected to the Tien River and extends 40 km eastward into PoR. The SSC reduction along the Hong Ngu channel differs in the different flood stages. In the rising stage, when the flow from the Tien River into the channel is not impaired by the secondary flood wave from the Cambodian floodplains and when floodplain inundation has not yet occurred in the VMD, SSC is reduced least of all flood stages. SSC in the channel changes considerably after the opening of the sluice gates. Sediment is trapped in the compartments and the return flow dilutes the already reduced SSC in the channels further. Now SSC is reduced rapidly over the first 10 km distance from the Tien River. At larger distances it remains stable at a very low level of around 20 $mg\,L^{-1}$. This corresponds well to the SSC reduction in the same channel measured in 2008 by Hung et al. (2014a).

The effect of the sluice gate opening on the flow dynamics in the channels is exemplarily illustrated for two nearby compartments in Fig. 8. It shows discharge and SSC of channels upstream and downstream of two sluice gates, as well as discharge and SSC flowing in and out of the compartments. After the opening of the sluice gates, the compartments are filled within 2–3 days. Then compartment 1 acts as a wide channel buffering the flow to the channel and to compartment 2. At the same time suspended sediment is entering the compartments and is deposited due to the reduced flow velocity. The outflow from compartment 1 with very low SSC dilutes the channel SSC. The diluted flow in the channel partly enters compartment 2, and flows further downstream the channel. This process is the primary reason of SSC reduction in the high and falling flood stages in the VMD.

5.3 Sedimentation and nutrient deposition in the VMD floodplains

Floodplain sedimentation is derived from the mass balance in every simulated compartment. The annual sedimentation rate is then calculated from the gross sedimentation per year and the floodplain area. The associated nutrient deposition is estimated from the sediment deposition rate by the average total nutrient proportion of the deposited sediment of 6.7 % (Manh et al., 2013). This proportion quantifies the summed deposition of total nitrogen, total phosphor, total potassium and total organic carbon. Finally, the sediment deposition depth is calculated from the cumulative sedimentation rate and the 1.2 $t\,m^{-3}$ dry bulk density of sediment soil in the MD specified in Xue et al. (2010).

A comparison of simulated sedimentation with measured data in 2011 (Manh et al., 2013) and in 2009 and 2010 (Hung et al., 2014b) is shown in Fig. 4c. A general tendency of the model to underestimate the monitored deposition can be observed. The underestimation is particularly pronounced for the high flood 2011. Here in 9 of 11 locations the simulated deposition is below the lower 95 % confidence bound associated to the measurement data (Manh et al., 2013). This underestimation is likely a consequence of different reasons:

1. In the floodplains the sediment grain size is very fine and small disturbances can already cause erosion and re-suspension. Hung et al. (2014b) showed that erosion occurs locally in the floodplains. Further, the settling velocity depends on the water temperature (Hung et al., 2014b). These effects are not described in the large-scale model.

2. The study focuses on the sediment delivered to the MD from the Mekong watershed. Erosion and re-suspension are ignored in the model setup by using a very high critical erosion shear stress for the whole model domain. Hence, the large amount of erosion from bed layers of channels is not considered and the sediment input to the floodplain compartments is smaller in the simulation than in reality. In the floodplain compartments, the eroded sediment settles again within the compartment due to the small flow velocities. Overall, this leads to significantly smaller simulated sedimentation rates.

3. Most of the sluice gates are operated by land owners using sandbags. The uncertainty and variability inherent in the dike levels and sluice gate operation might impact the simulation of floodplain deposition.

Despite this underestimation, the simulations are valuable, because they quantify the deposition of the newly arriving sediment to the VMD, excluding the local re-suspension and erosion. In addition, the model enables an analysis of the spatial distribution and variability of sediment deposition over the whole MD.

Table 4 lists the cumulative sediment and nutrient deposition for the regions PoR, LXQ and THA) and over the Vietnamese floodplains. The total sediment deposition in VMD varies from 0.43 mil. ton for the low flood year 2010 to 6.56 mil. ton for the extreme flood 2011. This is equivalent 1–6 % of the total sediment load at Kratie, respectively. The majority of the sediment is deposited in PoR (58–68 %), while THA receives only 8–14 %. The deposition in LXQ varies less and amounts to 23–28 %. This is explained by the smaller floodplain area in THA, and by the high number of high dike compartments in THA. The relative proportion of sediment deposition rises from 58 % in 2009

to 68 % in 2010 in PoR, while it reduces from 28 to 23 % in LXQ and 14 to 8 % in THA, respectively. The smaller fraction of high dike compartments in PoR leads to higher relative sedimentation in the low flood event 2010 compared to the normal and extreme flood years.

Since the nutrient deposition is directly linked to sedimentation, the pattern of nutrient deposition is identical to the sedimentation pattern. For the extreme flood 2011, 292×10^3 t, 102×10^3 t and 45×10^3 t of nutrients are deposited in PoR, LXQ and THA, respectively.

Table 4 also gives the spatial variability of sedimentation rates, nutrient rates and sediment depths for the three floods. This result basically depicts the effect of higher deposition in large flood events due to higher SSC, larger inundation extent and longer duration of compartment inundation. The range of sedimentation rates over the whole VMD in 2011 is 0.1–58 $\mathrm{kg\,m^{-2}yr^{-1}}$, while it is just 0.01–6.8 $\mathrm{kg\,m^{-2}\,yr^{-1}}$ in 2010. This large range of deposition for a given flood season illustrates the very high spatial variability, and can be explained by the very different distances to the main sediment sources and the heterogeneous opening times of sluice gates. The mean deposition in THA is considerably higher than in the other regions, because the distances to main rivers never exceed 10 km. In summary, the average sedimentation rates are 0.36, 1.02, and 2.1 $\mathrm{kgm^{-2}\,yr^{-1}}$ in the low, normal and extreme flood, respectively, with average nutrient deposition of 24, 68, and 141 $\mathrm{g\,m^{-2}\,yr^{-1}}$, and sedimentation depths of 0.3, 0.9 and 1.7 mm.

In order to quantify the benefit of nutrient deposition in inundated compartments, we compare the cumulative nutrient deposition rate with the average total amount of N, P, K fertilizers that is applied to rice crops in the wet season (Khuong et al., 2007). The cost of fertilizers and pesticides amount to approximately 40 and 15 % of the total costs per rice crop season (Thong al et., 2011; Phuong and Xe, 2011). Table 5 shows the average N, P, K deposition in floodplains and the N, P, K requirements for a rice crop. Depending on the event, the floods supply 13–75 % N, 10–58 % P, and 145–835 % K to the floodplains. In the normal flood 2009 flooding can provide more than 50 % of

the typically applied rice crop fertilizers. This is a significant reduction of the costs for mineral fertilizers compare to high dike compartments.

Figure 9 (top row panels) shows the spatial variability of the sedimentation rate in the VMD floodplains over the flood season 2009. These maps are interpolated using Kriging based on the deposition rates of the 1-D representation of the floodplains in the hydrodynamic model. In middle September a number of sluice gates are opened or overtopped. These are mostly located along the border of Vietnam to Cambodia, where the water levels rise first. During this period the daily sedimentation rates are quite high because of high SSC of the channel water flowing into the floodplain compartments. In middle October all the low dike compartments and some high dike compartments are overtopped or opened, i.e. a large proportion of the floodplains is inundated. The daily sedimentation rates during this peak discharge period are very high, especially in the vicinity of the Tien and Hau Rivers and the border channels. In PoR almost all compartments are inundated and trap sediment, but the sedimentation rates reduce with distance from the Tien River and the border channel. Thus the deposition rate becomes quite low in the southern part of PoR. In THA most of the compartments are closed and the high dikes prevent inundation during the peak discharge. Sedimentation occurs only in some compartments along the border and close to the rivers. In these compartments the deposition rate is very high. Similarly, sediment deposition cannot occur in the central part of LXQ, where a large number of high dike compartments exist and the sluice gates remain closed during the high flood period. Like in THA, sedimentation in LXQ is mainly concentrated along the border and in close proximity of the Hau River. At the end of November the flood is receding in the upper part of the VMD and many compartments are closed to start a new crop season. The patterns of the sedimentation rates are similar to those in September, but with much lower rates.

The bottom row of Fig. 9 shows maps of the annual deposition for the simulated flood events. In the extreme flood 2011, the inundated area is not much larger than inundation in the normal flood 2009, but the sedimentation rates differ strongly. The total sedimentation in 2011 is more than three times the deposition in 2009 (cf. also

Table 4). This is the result of the higher flood magnitude and longer flood duration. The opposite holds true for the extremely low flood 2010: low water levels and short inundation duration allow only very low sediment deposition. The total sedimentation rate is just 19 and 6 % of the total rate in the normal and extreme year, respectively. The sedimentation in the low flood year is mostly concentrated in the compartments close to the border channels and main rivers. No sediment deposition occurs in the central LXQ and very little sediment is trapped in central PoR. Figure 9 (bottom row panels) also shows the differences between measured and modeled sedimentation (vertical bars). The smallest differences are observed in upper PoR, where the sampling locations are closer to the sediment sources, i.e. Tien River and overland flow from Cambodia. In the remote areas in PoR and LXQ the transported SSC is very small as Figs. 6 and 7 illustrate. The main sediment source is local erosion in channels and floodplains, which should be the major source for the differences between measured and simulated sedimentation.

6 Conclusions

This study presents a comprehensive approach to quantify the suspended sediment and sediment-related nutrient transport and deposition in the whole MD. The intricate system of rivers, channels and floodplains, including control structures and human interventions such as sluice gate operation, is described by a quasi-2-D model linking a hydrodynamic and a cohesive sediment transport model. The two-stage, automatic calibration approach uses six objective functions. In that way, different types of observed information are taken into account with the aim to obtain the best possible representation of the large-scale water and sediment transport by the simulation. The good agreement between observations and model results shows that the large-scale quantification of water and sediment transport for the MD is possible with reasonable effort. It can be concluded that, for the first time, a large-scale quantification of sediment and sediment-related nutrient transport for the whole MD has been achieved.

The model considers only the sediment transport originating from the Mekong basin and entering the MD at Kratie. Re-suspension and erosion in channels and floodplains are not included. As a consequence, the simulations tend to underestimate sedimentation in the floodplains. This effect is particularly pronounced in the remote areas of the VMD (PoR and LXQ). Here, we have very small sediment concentrations, and hence, re-mobilization is more important compared to regions closer to the main rivers and channels. Sediment re-mobilization is highly influenced by human activities; the understanding and quantification of these processes require further field investigations.

The model provides the spatial and temporal variation of the suspended sediment transport and sediment-nutrient deposition from Kratie at the entrance of the MD to the coast. A very high variability of floodplain sedimentation is given in the VMD. Higher rates occur in closer distances to sediment sources. During the rising flood stage no sedimentation in floodplains occurs due to closed sluice gates. The channel network is very effective in transporting sediment, also deeply into the remote floodplain areas. In the flood peak stage flood water can enter compartments and sediment deposition is initiated. The outflow from compartments dilutes SSC in the channels, which causes in turn a high heterogeneity of SSC in the dense channel network of the VMD. Further, SSC becomes very small with larger distances from the sediment sources which contributes to the very high variability of floodplain sedimentation.

In order to achieve higher sediment deposition with a lower variability across the VMD, the following recommendations can be deduced from our findings: (1) the overflow of the border channels with low SSC which now enter the VMD floodplains should be tranferred, by increasing the capacity of the border channels, either to Vam Co River in PoR, or to the West Sea in LXQ. This would enable flow with high SSC from Tien River and Hau River to the lower part of the floodplains. (2) The channels starting from Tien River and Hau River should be enlarged to be able to convey higher sediment mass. (3) From a management point of view, crop schedules in PoR and LXQ should be adapted to keep sluice gates open for longer periods, and compartments/sluice gates in larger distance to sediment sources should be opened earlier than the nearer

compartments. Optimizing the operation of sluice gates is the best solution to transport and trap sediment in the floodplain compartments in PoR and LXQ in the VMD.

Sediment transport and deposition are significantly different for the simulated flood seasons. With higher flood magnitudes the impact of the buffering by the Tonle Sap Lake and the Cambodian floodplains on the flood quantity in VMD is larger. 57–68 % of the total sediment load in Kratie is transported to VMD (Tan Chau and Chau Doc) in the different simulated years, while this proportion is reduced to 48–57 % in the coastal zones at Can Tho and My Thuan. Floodplain deposition is, as expected, higher with higher flood magnitudes. 11.5–15 % of the total sediment load in Kratie is transported to VMD, of which only 1.0–6.3 % is trapped in floodplain compartments. This amounts to 0.36–2.10 $kg\,m^{-2}\,yr^{-1}$, which is equivalent to 24–141 g of total nutrients (N, P, K) per $m^2\,yr^{-1}$, and to a sediment deposition on the floodplains of 0.3–1.7 mm soil layer per year. The mean N, P, K deposition is equivalent to 36 % total nitrogen (N), 28 % total phosphor (P), 400 % total potassium (K) of mineral fertilizers typically used in high ring dike systems.

Our quantification could be used to assess the nutrient deficit caused by fully flood controlled dike systems in the VMD. It would allow a cost-benefit analysis of natural inundation vs. dike construction and implementation of three crops per year. Further, it shows that the Mekong River basin is a net contributor of sediment to the MD. The annual deposited soil layer of 0.3–1.7 mm is a significant counterbalance to the land subsidence in the MD, estimated to 6 $mm\,yr^{-1}$ (Syvitski al et., 2009). Our model could also be used to quantify the future impacts of the planned and ongoing dam construction and of the ongoing sea level rise on the sediment transport in the MD.

Acknowledgements. This work was performed within the project WISDOM – Water related Information System for a Sustainable Development of the Mekong Delta (www.wisdom.eoc.dlr.de). Funding by the German Ministry of Education and Research (BMBF) and support by the Vietnamese Ministry of Science and Technology (MOST) within the framework of National project coded KC08.21/11-15 are gratefully acknowledged. We also appreciate the provision of sediment data for stations in Cambodia by Matti Kummu.

The service charges for this open access publication
have been covered by a Research Centre of the
Helmholtz Association.

References

Abbott, M. B. and Ionescu, F.: On the numerical computation of nearly-horizontal flows, J. Hydraul. Eng., 5, 97–117, 1967.

Droppo, I. G.: Rethinking what constitutes suspended sediment, Hydrol. Process., 15, 1551–1564, doi:10.1002/hyp.228, 2001.

Dung, N. V., Merz, B., Bárdossy, A., Thang, T. D., and Apel, H.: Multi-objective automatic calibration of hydrodynamic models utilizing inundation maps and gauge data, Hydrol. Earth Syst. Sci., 15, 1339–1354, doi:10.5194/hess-15-1339-2011, 2011.

Ericson, J., Vorosmarty, C., Dingman, S., Ward, L., and Meybeck, M.: Effective sea-level rise and deltas: causes of change and human dimension implications, Global Planet. Change, 50, 63–82, doi:10.1016/j.gloplacha.2005.07.004, 2006.

Fu, K. D. and He, D. M.: Analysis and prediction of sediment trapping efficiencies of the reservoirs in the mainstream of the Lancang River, Chinese Sci. Bull., 52, 134–140, doi:10.1007/s11434-007-7026-0, 2007.

Fu, K. D., He, D. M., and Lu, X. X.: Sedimentation in the Manwan reservoir in the Upper Mekong and its downstream impacts, Quatern. Int., 186, 91–99, doi:10.1016/j.quaint.2007.09.041, 2008.

Gupta, A.: Large Rivers: Geomorphology and Management, John Wiley & Sons Ltd., The Atrium, Southern Gate, Chichester, West Sussex, England, 2008.

Gupta, H., Kao, S.-J., and Dai, M.: The role of mega dams in reducing sediment fluxes: a case study of large Asian rivers, J. Hydrol., 464–465, 447–458, doi:10.1016/j.jhydrol.2012.07.038, 2012.

Heege, T., Kiselev, V., Wettle, M., and Hung, N. N.: Operational multi-sensor monitoring of turbidity for the entire Mekong Delta, Int. J. Remote Sens., 35, 2910–2926, doi:10.1080/01431161.2014.890300, 2014.

Hung, N. N., Delgado, J. M., Tri, V. K., Hung, L. M., Merz, B., Bárdossy, A., and Apel, H.: Floodplain hydrology of the Mekong Delta, Vietnam, Hydrol. Process., 26, 674–686, doi:10.1002/hyp.8183, 2012.

Hung, N. N., Delgado, J. M., Güntner, A., Merz, B., Bárdossy, A., and Apel, H.: Sedimentation in the floodplains of the Mekong Delta, Vietnam, Part II: deposition and erosion, Hydrol. Process., 28, 3145–3160, doi:10.1002/hyp.9855, 2014a.

Hung, N. N., Delgado, J. M., Güntner, A., Merz, B., Bárdossy, A., and Apel, H.: Sedimentation in the floodplains of the Mekong Delta, Vietnam, Part I: suspended sediment dynamics, Hydrol. Process., 28, 3132–3144, doi:10.1002/hyp.9856, 2014b.

Kashefipour, S. M. and Falconer, R. A.: Longitudinal dispersion coefficients in natural channels, Water Res., 36, 1596–1608, 2002.

Khuong, T. Q., Thi, T., Huan, N., Tan, P. S., and Buresh, R.: Effect of site specific nutrient management on grain yield, nutrient use efficiency and rice production profit in the Mekong Delta, Omonrice, 158, 153–158, 2007.

Kuenzer, C., Guo, H., Huth, J., Leinenkugel, P., Li, X., and Dech, S.: Flood mapping and flood dynamics of the Mekong Delta: ENVISAT-ASAR-WSM based time series analyses, Remote Sens., 5, 687–715, doi:10.3390/rs5020687, 2013.

Kummu, M. and Varis, O.: Sediment-related impacts due to upstream reservoir trapping, the Lower Mekong River, Geomorphology, 85, 275–293, doi:10.1016/j.geomorph.2006.03.024, 2007.

Kummu, M., Penny, D., Sarkkula, J., and Koponen, J.: Sediment: curse or blessing for Tonle Sap Lake?, Ambio, 37, 158–163, 2008.

Kummu, M., Lu, X. X., Wang, J. J., and Varis, O.: Basin-wide sediment trapping efficiency of emerging reservoirs along the Mekong, Geomorphology, 119, 181–197, doi:10.1016/j.geomorph.2010.03.018, 2010.

Kummu, M., Tes, S., Yin, S., Adamson, P., Józsa, J., Koponen, J., Richey, J. and Sarkkula, J.: Water balance analysis for the Tonle Sap Lake-floodplain system, Hydrol. Process., 28, 1722–1733, doi:10.1002/hyp.9718, 2014.

Leinenkugel, P., Kuenzer, C., Oppelt, N., and Dech, S.: Characterisation of land surface phenology and land cover based on moderate resolution satellite data in cloud prone areas – a novel product for the Mekong Basin, Remote Sens. Environ., 136, 180–198, doi:10.1016/j.rse.2013.05.004, 2013.

Liu, C., He, Y., Walling, E., and Wang, J.: Changes in the sediment load of the Lancang-Mekong River over the period 1965–2003, Sci. China Technol. Sci., 56, 843–852, doi:10.1007/s11431-013-5162-0, 2013.
Liu, X. and He, D.: A new assessment method for comprehensive impact of hydropower development on runoff and sediment changes, J. Geogr. Sci., 22, 1034–1044, doi:10.1007/s11442-012-0981-7, 2012.
Lu, X. X. and Siew, R. Y.: Water discharge and sediment flux changes over the past decades in the Lower Mekong River: possible impacts of the Chinese dams, Hydrol. Earth Syst. Sci., 10, 181–195, doi:10.5194/hess-10-181-2006, 2006.
Lu, X., Kummu, M., and Oeurng, C.: Reappraisal of sediment dynamics in the Lower Mekong River, Cambodia, Earth Surf. Proc. Land., doi:10.1002/esp.3573, in press, 2014.
Manh, N. V., Merz, B., and Apel, H.: Sedimentation monitoring including uncertainty analysis in complex floodplains: a case study in the Mekong Delta, Hydrol. Earth Syst. Sci., 17, 3039–3057, doi:10.5194/hess-17-3039-2013, 2013.
Mike11: Reference Manual: A Modelling System for Rivers and Channels, available from: http://www.mikebydhi.com/ (last access: 15 April 2014), 2012.
Milliman, J. D. and Farnsworth, K. L.: River Discharge to the Coastal Ocean: a Global Synthesis, Cambridge University Press, 2011.
MRC: Annual Mekong Flood Report 2006, Mekong River Comm., 1–94, available from: http://www.mrcmekong.org/assets/Publications/basin-reports/Annual-Mekong-Flood-Report-2006.pdf (last access: 15 April 2014), 2007.
MRC: The Flow of the Mekong, Mekong River Comm., 1–12, available from: http://www.mrcmekong.org/assets/Publications/report-management-develop/MRC-IM-No2-the-flow-of-the-mekong.pdf (last access: 15 April 2014), 2009.
MRC: Annual Mekong Flood Report 2009, Mekong River Comm., 1–95, available from: http://www.mrcmekong.org/assets/Publications/basin-reports/Annual-Mekong-Flood-Report-2009.pdf (last access: 15 April 2014), 2010.
MRC: Annual Mekong Flood Report 2010, Mekong River Comm., 1–76, available from: http://www.mrcmekong.org/assets/Publications/basin-reports/Annual-Mekong-Flood-Report-2010.pdf (last access: 15 April 2014), 2011a.
MRC: MRC Technical Paper: Flood Situation Report 2011, Mekong River Comm., 1–59, available from: http://www.mrcmekong.org/assets/Publications/technical/Tech-No36-Flood-Situation-Report2011.pdf (last access: 15 April 2014), 2011b.

MRC/DMS: Origin, fate and impacts of the Mekong sediments, Mekong River Comm., 53, available from: http://www.mpowernetwork.org/Knowledge_Bank/Key_Reports/PDF/Research_Reports/DMS_Sediment_Report.pdf (last access: 15 April 2014), 2009.
MRCS/WUP-FIN report: Research findings and recommendations, Mekong River Comm., available from: http://wacc.edu.vn/vi/wp-content/uploads/2013/06/wup-fin2_final-report_part2.pdf (last access: 15 April 2014), 2007.
Phuong, D. T. K. and Xe, D. V.: Assessment for efficiency finance of rice monoculture and rice – upland crops systems at Cai Lay district, Tien Giang province, J. Sci.-CTU, 18a, 220–227, 2011.
Syvitski, J. P. M. and Higgins, S.: Going under: the world's sinking deltas, New Sci., 216, 40–43, doi:10.1016/S0262-4079(12)63083-8, 2012.
Syvitski, J. P. M. and Saito, Y.: Morphodynamics of deltas under the influence of humans, Global Planet. Change, 57, 261–282, doi:10.1016/j.gloplacha.2006.12.001, 2007.
Syvitski, J. P. M., Kettner, A. J., Overeem, I., Hutton, E. W. H., Hannon, M. T., Brakenridge, G. R., Day, J., Vörösmarty, C., Saito, Y., Giosan, L., and Nicholls, R. J.: Sinking deltas due to human activities, Nat. Geosci., 2, 681–686, doi:10.1038/ngeo629, 2009.
Thong, P. Le, Xuan, H. T. D., and Duyen, T. T. T.: Economic efficiency of summer–autumn and autumn–spring rice crop in the Mekong River Delta, J. Sci.-CTU, 18, 267–276, 2011.
Thuyen, L. X., Tran, H. N., Tuan, B. D., and Bay, N. T.: Transportation and deposition of fine sediment during flood season in Long Xuyen Quadrangle – Technical Report (Vietnamese), Minist. Sci. Technol., 1–70, 2000.
Ve, N. B.: Assessment of sustainability of 3 rice crops in the Vietnamese Mekong Delta (Vietnamese), Three rice Crop. Work., An Giang, Vietnam, 1–8, 2009.
Vien, D. M., Binh, V. V, Huong, H. T., and Guong, V. T.: The impact of flood sediments on rice yield and soil fertility in the Mekong River Delta (Vietnamese), J. Sci.-CTU, 1–11, 2011.
Walling, D. E.: Evaluation and analysis of sediment data from the lower Mekong River (Report), available from: http://portal.mrcmekong.org/master-catalogue/search?giai=9506000003825_00011452E0100jdi (last access: 15 April 2014), 2005.
Walling, D. E.: The changing sediment load of the Mekong River, Ambio, 37, 150–157, 2008.
Wolanski, E., Huan, N. N., Dao, L. T., Nhan, N. H., and Thuy, N. N.: Fine-sediment dynamics in the Mekong River Estuary, Vietnam, Estuar. Coast. Shelf Sci., 43, 565–582, doi:10.1006/ecss.1996.0088, 1996.

Xue, Z., Liu, J. P., DeMaster, D., Van Nguyen, L., and Ta, T. K. O.: Late Holocene evolution of the Mekong Subaqueous Delta, Southern Vietnam, Mar. Geol., 269, 46–60, doi:10.1016/j.margeo.2009.12.005, 2010.

Table 1. The calibration parameters and the calibration zones: manning roughness coefficient (n), dispersion factor (a), critical deposition shear stress $\tau_{c,b}$ ($N m^{-2}$) and free settling velocity W_0($m s^{-1}$). Least Euclidian distance parameters (O) and fixed parameters (F).

Zone	n	a	$\tau_{c,d}$	W_0	Description
1	0.032 O	400 F	0.025 F	2.5×10^{-4} F	Mekong River: Kratie to Phnom Penh
2	0.031 O	500 F	0.025 F	2.5×10^{-4} F	Mekong River: Phnom Penh to border
3	0.036 O	50 F	0.025 F	1×10^{-4} O	Cambodian floodplains
4	0.030 O	500 F	0.025 F	2.5×10^{-4} F	Tien River: Border to My Thuan
5	0.026 O	700 F	0.025 F	2.5×10^{-4} F	Tien River: My Thuan to coast
6	0.027 O	500 F	0.025 F	2.5×10^{-4} F	Hau River: Border to Can Tho
7	0.024 O	700 F	0.025 F	2.5×10^{-4} F	Hau River: Can Tho to coast
8	0.034 O	335 O	0.021 O	1×10^{-4} O	VMD channels with $Q > 100\,m^3\,s^{-1}$
9	0.025 O				VMD channels with $Q \leq 100\,m^3\,s^{-1}$
10	0.018 O	50 F	0.190 O	8×10^{-4} O	VMD floodplains
11	0.016 F	831 O	0.025 F	2.5×10^{-4} F	Coastal zones

Table 2. Model performance: calibration objectives, data used (number of locations and number of data points), results of calibration (for the year 2011) and of validation (for the years 2009 and 2010).

Objectives	No. of stations/ no. of data	Calibration (2011)			Validation (2009/2010)		
		NSE	FAI	RMSE	NSE	FAI	RMSE
H (m)	13/daily	0.84	–	–	0.74/no data	–	–
Q ($m^3 s^{-1}$)	10/daily	0.63	–	–	0.51/0.74	–	–
Inundation	571/17	–	0.46	–	–	0.39/0.36	–
River SSC ($mg L^{-1}$)	2/daily	0.52	–	–	0.2[1]/0.78	–	–
Channel SSC ($mg L^{-1}$)	79/6	–	–	40	–	–	60/no data
Sedimentation ($kg m^{-2} yr^{-1}$)	11/–	–	–	8.55/ [4.4–18.8][2]	–	–	5.27/1.28
					–	–	–

[1] in which NSE = 0.9 at Tan Chau and NSE = −0.56 at Chau Doc
[2] is the RMSE calculated against the mean 95 % CI of the measured deposition

Table 3. Total sediment load, flood volume and relative sediment load (with reference to Kratie) at key locations in the MD for three flood events.

Subsystem	Sediment load (mil. ton)			Sediment load (%)			Flood volume (%)		
	2009	2010	2011	2009	2010	2011	2009	2010	2011
Kratie	78.4	43.4	104.2	100 %	100 %	100 %	100 %	100 %	100 %
Cam floodplains	21.4	10.3	27.3	27 %	24 %	26 %	11 %	9 %	16 %
Overflow to VN	3.5	1.5	7.0	4 %	4 %	7 %	6 %	4 %	9 %
Tonle Sap Lake	5.2	2.1	10.6	7 %	5 %	10 %	8 %	6 %	12 %
Vietnamese MD	51.8	31.0	66.3	66 %	71 %	64 %	92 %	93 %	86 %
Tan Chau	41.0	24.7	50.3	52 %	57 %	48 %	67 %	70 %	60 %
Chau Doc	7.3	4.7	9.0	9 %	11 %	9 %	19 %	19 %	18 %
Vam Nao	14.7	9.3	18.7	19 %	21 %	18 %	26 %	28 %	23 %
VN floodplains	10.9	5.6	17.6	14 %	13 %	17 %	21 %	17 %	24 %
Deposited in compartments	2.3	0.4	6.6	3 %	1 %	6 %	–	–	–
Coast	42.0	25.9	50.5	54 %	60 %	48 %	–	–	–

Table 4. Cumulative sediment and nutrient deposition mass in different spatial units (absolute mass and relative to Kratie). The variability of sedimentation rate, deposition depths and nutrient deposition rates in the VMD.

Zone	Item	Unit	2009	2010	2011
VMD	Sedimentation	10^6 t	2.27	0.43	6.56
VMD	Nutrients	10^3 t	152.5	28.8	439.9
PoR	Sedimentation & Nutrients	PoR/VMD	58 %	68 %	66 %
LXQ		LXQ/VMD	28 %	23 %	23 %
THA		THA/VMD	14 %	8 %	10 %
VMD	Sedimentation ($kg\,m^{-2}$)	Min	0.05	0.01	0.10
		Mean	1.02	0.36	2.10
		Max	27.2	6.85	58.44
	Depth	(mm)	0.90	0.30	1.80
	Nutrients	($g\,m^{-2}$)	68.5	24.4	141.0

Table 5. Mean nutrients supply from flood events to floodplains and nutrient need for a rice crop in the wet season.

Event	N ($kg\,ha^{-1}$)		P ($kg\,ha^{-1}$)		K ($kg\,ha^{-1}$)	
2009	33.6	36 %	13.0	28 %	154.2	406 %
2010	12.0	13 %	4.6	10 %	55.0	145 %
2011	69.1	75 %	26.8	58 %	317.2	835 %
required	92.1		46.0		38.0	

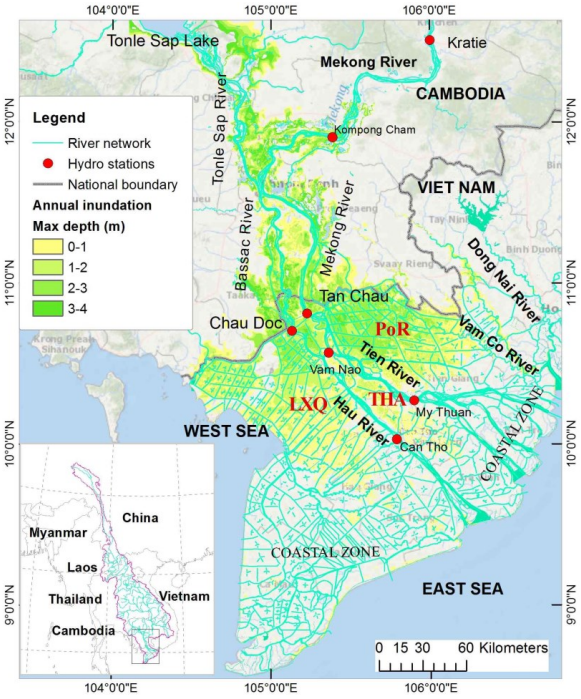

Fig. 1. The Mekong Delta from Kratie to the coasts, including the river networks, main discharge stations and the inundated area (average over 10 yr).

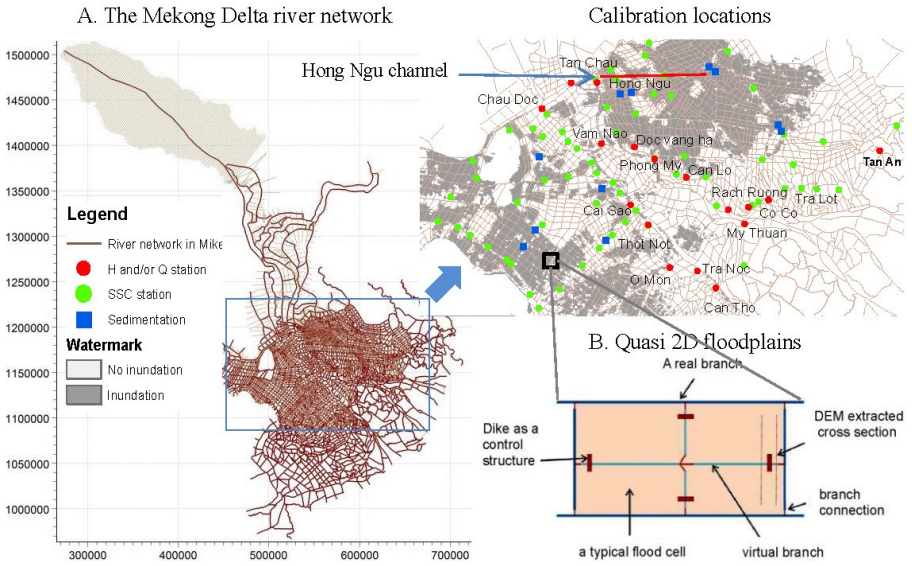

Fig. 2. (A) The model river network and the calibration locations. **(B)** Quasi-2-D concept for a typical floodplain compartment in the VMD.

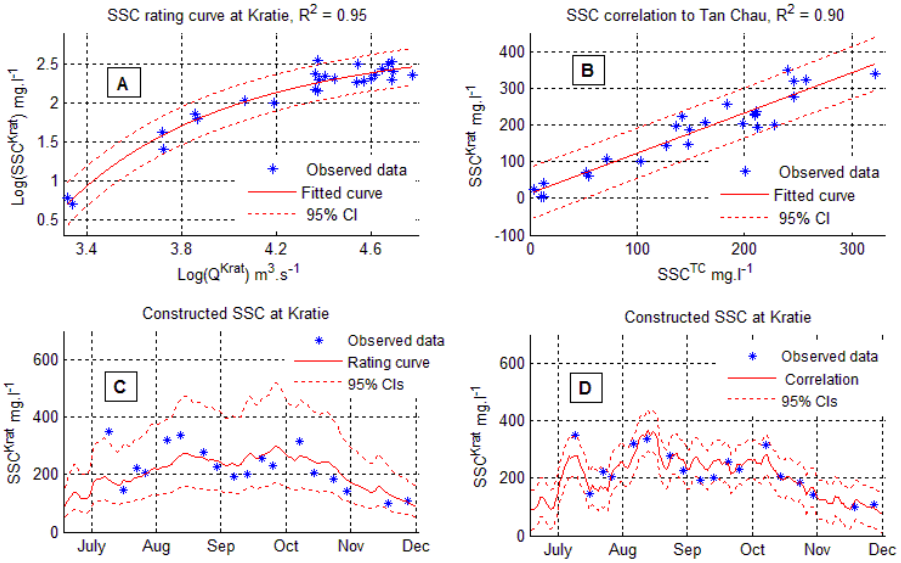

Fig. 3. (A) Derived SSC for Kratie using sediment rating curve, **(B)** derived SSC for Kratie using correlation to SSC at Tan Chau, **(C)** comparison of sediment rating curve method with measured data in 2011, **(D)** comparison of correlation method with measured data in 2011.

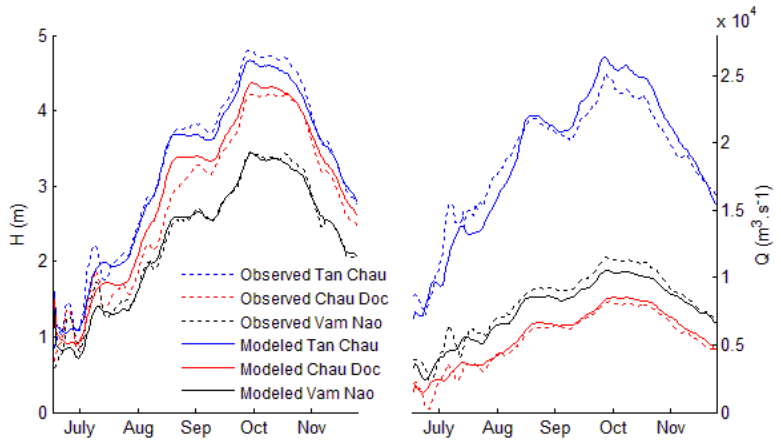

Fig. 4a. Comparison of measurements and simulation results at stations Tan Chau, Chau Doc and Vam Nao for 2011: daily water levels (left panel), daily discharges (right panel).

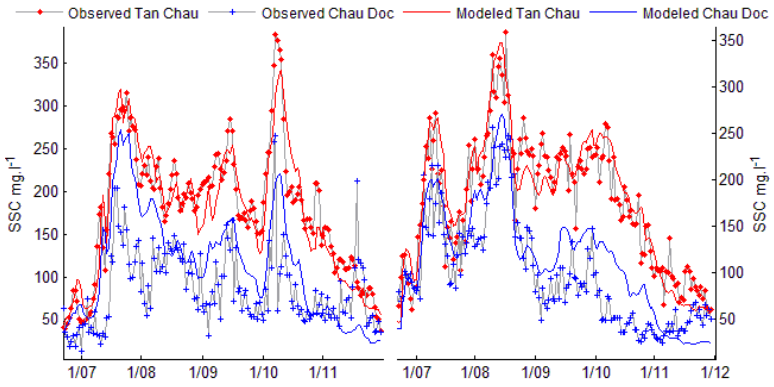

Fig. 4b. Comparison of measurements and simulation results at Tan Chau and Chau Doc: daily SSC for the calibration year 2011 (right panel) and for the validation year 2009 (left panel).

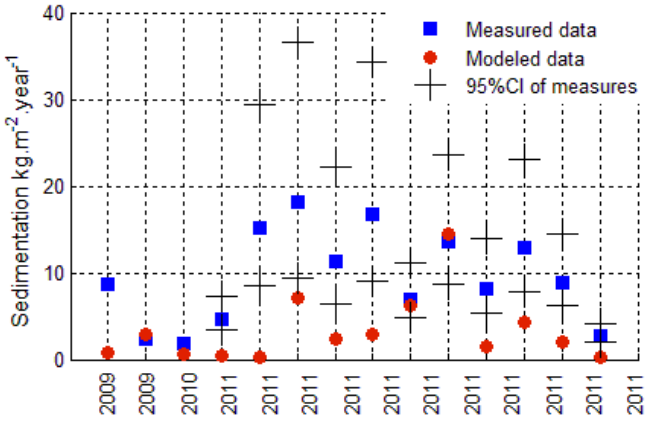

Fig. 4c. Comparison of measured and simulated sedimentation (2 locations in 2009, 1 location in 2010, 11 locations in 2011).

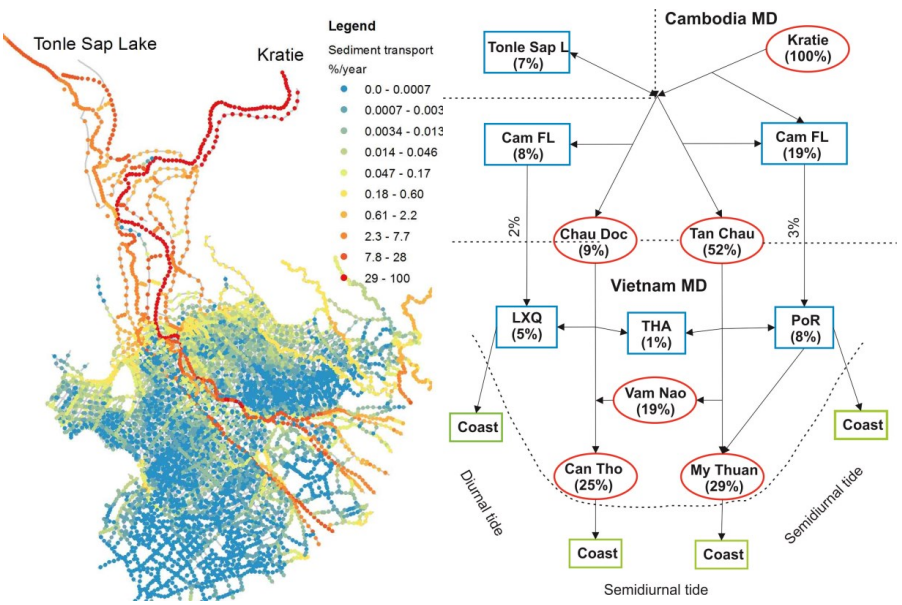

Fig. 5. Proportion of transported sediment in the whole MD compared to sediment load at Kratie (left panel). Sediment load transport into subsystems (green blocks) and to key stations (red circles) for the year 2009 (right panel).

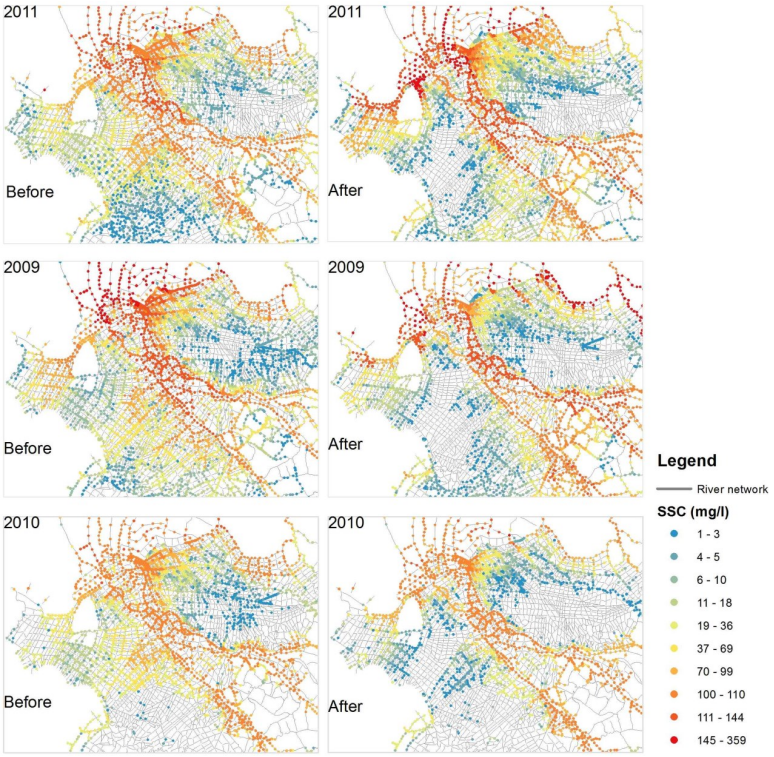

Fig. 6. SSC distribution in the VMD for three floods: SSC distribution before (left panels) and after (right panels) sluice gate opening.

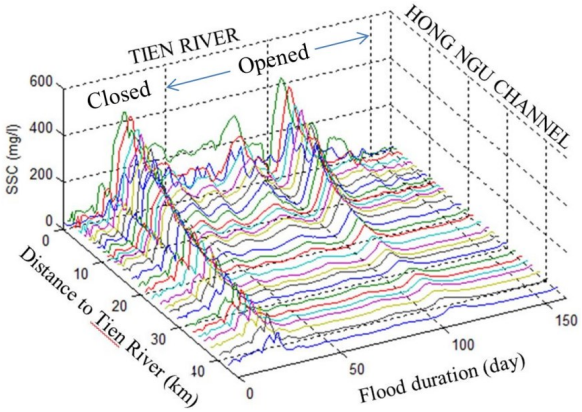

Fig. 7. Typical SSC reduction in the channels with distance to the main river in the Plain of Reeds, exemplarily shown for the Hong Ngu channel in 2011.

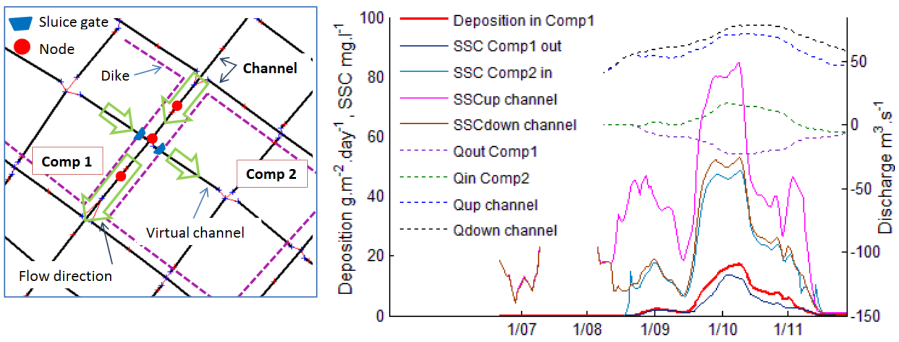

Fig. 8. Flow direction in channels and two nearby compartments (left panel). Discharge and sediment dynamics between a channel and two nearby compartments and sediment deposition in compartment 1 for 2011 (right panel).

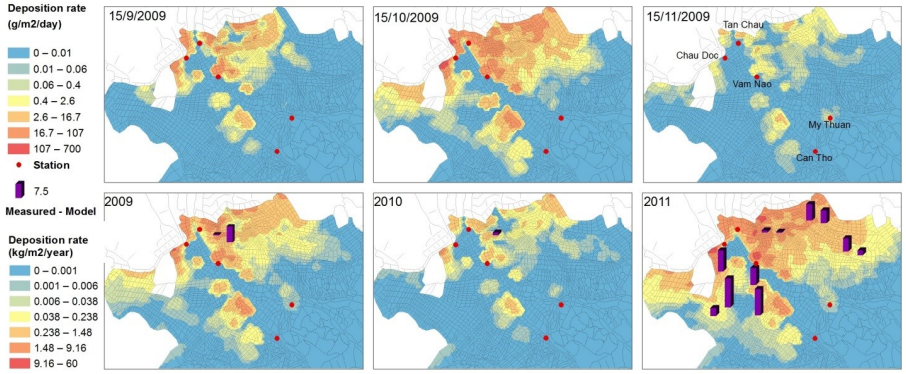

Fig. 9. Map of sedimentation in the VMD floodplains. Top panels: sediment deposition rate ($g\,m^{-2}\,day^{-1}$) during the period of compartment opening (left panel), during flood peak discharge (center panel) and during the period of compartment closing (right panel). Bottom panels: cumulative sediment deposition ($kg\,m^{-2}\,yr^{-1}$) in 2009, 2010 and 2011. The bars show the differences of cumulative sediment deposition between measurements and simulation.